

# A novel configuration of a microstrip metamaterial reconfigurable bandstop filter

Amina Aghanim<sup>1</sup>, Otman Oulhaj<sup>1</sup>, Jamal Zbitou<sup>2,3</sup>, Aziz Oukaira<sup>4</sup>, Ahmed Lakhssassi<sup>4,5</sup>, Rafik Lasri<sup>1</sup>

<sup>1</sup>TEDAEEP Research Team, Faculty Polydisciplinary Larache, Abdelmalek Essaâdi University, Tetouan, Morocco

<sup>2</sup>Laboratory of Information and Communication Technologies (LabTIC), National School of Applied Sciences (ENSA) Tangier, Abdelmalek Essaâdi University, Tetouan, Morocco

<sup>3</sup>National School of Applied Sciences of Tetouan (ENSATe), Abdelmalek Essaâdi University, Tetouan, Morocco

<sup>4</sup>Department of Electrical and Computer Engineering, University of Quebec, Outaouais, Canada

<sup>5</sup>Department of Electrical and Computer Engineering, University of Sherbrooke, Sherbrooke, Canada

## Article Info

### Article history:

Received Dec 28, 2023

Revised Apr 2, 2024

Accepted Apr 16, 2024

### Keywords:

Filter

Reconfigurable

Split ring resonator

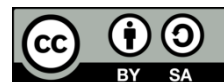
Stopband

Varactor

## ABSTRACT

This paper presents the design, simulation, and test measurements of a microstrip bandstop filter operating at 1.5 GHz, incorporating six split ring resonator (SRR) unit cells. The substrate employed is an FR-4 with a thickness of 1.6 mm and tangent losses of 0.025. In the initial phase, the design is conceptualized, simulated using computer simulation technology (CST) studio and advanced design system (ADS) Agilent simulators, and validated through test measurements. Building upon this foundation, the filter is transformed into a reconfigurable variant by integrating four SMV2019 varactor diodes. These varactors are modeled to ensure the reconfigurability of the bandwidth. The integration of varactors introduces dynamic tuning capabilities to the considered bandstop filter.

*This is an open access article under the [CC BY-SA](https://creativecommons.org/licenses/by-sa/4.0/) license.*



## Corresponding Author:

Amina Aghanim

TEDAEEP Research Team, Faculty Polydisciplinary Larache, Abdelmalek Essaâdi University

Tetouan, Morocco

Email: amina.aghanim@etu.uae.ac.ma

## 1. INTRODUCTION

The escalating demand in the radio frequency (RF) and microwave domain, fueled by applications in wireless communications, internet of things (IoT) technology, radar systems, and cognitive radio [1]–[5], has introduced challenges such as interferences and signal quality reduction. These issues saturate the frequency spectrum, hindering the optimal deployment of RF and microwave technologies. In response, advanced filtering mechanisms are imperative. RF bandstop filters, particularly in microstrip technology, emerge as a promising solution, offering flexibility for integration into compact devices while ensuring optimal filtering performance [6]. These filters are not only cost-effective but also easy to fabricate, addressing challenges in the development and deployment of RF and microwave technologies. Microstrip technology leverages metamaterial properties for the design of optimized bandstop filters [7]–[10]. Metamaterials, engineered with artificial complex geometries, yield unique properties, including negative permittivity and permeability. The historical development of metamaterials, from Veselago's theoretical work in 1986 to Pendry's introduction of the split ring resonator in 1999, laid the foundation for innovative approaches to RF filtering [11]–[13].

The recent focus on reconfigurable filters represents a significant shift from traditional static filters. Reconfigurability, achieved through continuous and discrete avenues, addresses crucial parameters such as bandwidth, center frequency, poles, zeros, and quality factors [14]–[16]. This pursuit is motivated by the

evolving landscape of wireless communication standards, requiring adaptability for seamless adjustment to new requirements without hardware replacements. Continuous reconfigurability involves dynamic adjustments using varactor diodes and micro electro mechanical system (MEMS) capacitors, providing swift tuning capabilities [4], [17], [18]. Varactor diodes, known for their compact dimensions and cost-effectiveness, offer advantages for achieving continuous reconfigurability. Discrete reconfigurability, on the other hand, involves distinct modifications using PIN diodes, MEMS switches, and optical frequency combs. Practical applications of reconfigurable filters, such as tunable microwave filters and innovative designs like  $\lambda/4$  and  $\lambda/2$  tunable filters and multi-mode filters, highlight reduced size and simple tuning circuitry appeal [19]–[22].

This study aims squarely at advancing the capabilities of split-ring resonators (SRR) to meet the evolving needs of wireless communication technologies. By incorporating the SMV2019 varactor diode into the stopband filter structure, we break through the limitations inherent in traditional tuning methods, enabling unprecedented control over frequency band and polarization. This development is essential for enhancing the resilience, reliability, and adaptability of communication systems across a spectrum of scenarios, aligning with the dynamic requirements of contemporary wireless standards. Through our comprehensive modeling in advanced design system (ADS) software, coupled with the introduction of an innovative polarization circuit, we demonstrate significant enhancements in SRR functionality.

## 2. IMPLEMENTATION OF A BANDSTOP FILTER WITH SRR

### 2.1. SRR unit cell

The SRR comprises two embedded rings, each split on opposite sides. The resonant wavelength of the SRR structure exceeds the diameters of the rings due to the gap between the outer and inner rings as illustrated in Figures 1(a) and 1(b). The resonance frequency of an SRR is influenced by two primary factors: substrate permittivity and resonator length [23], [24]. To ensure effective coupling, minimizing the distance between the rings and the line is crucial, creating a negative medium and exhibiting bandstop performances. This frequency inhibition effect is intrinsic to the SRR structure, which can be equated to an equivalent circuit combining two capacitances,  $C_{gap}$ ,  $C_m$  and an inductance  $L_m$  as depicted in Figure 1 (c). Equations (1) to (4) represent the formulas for calculating the parameters of the capacitance and the inductance [7].

$$C_m = \frac{A\varepsilon_0\varepsilon_r(2L_1+2L_2-G)}{2s} \quad (1)$$

$$C_{gap} = \frac{\varepsilon_0\varepsilon_r t_c}{G} \quad (2)$$

$$L_m = \frac{\mu_0 s(L_1+L_2)}{W} \quad (3)$$

$$A = \frac{c^2}{4\pi^2(L_1+L_2)^2 f_0 \varepsilon_r} \quad (4)$$

where:  $\varepsilon_0$  is the vacuum permittivity,  $\varepsilon_r$  is the relative dielectric permittivity,  $\mu_0$  is the vacuum permeability,  $L_1$ , and  $L_2$  represent the outer and inner lengths of the rings. The approach of Nicolson Ross Weir verifies the metamaterial characteristic of the unit cell of an SRR. This approach rests on the sum and subtraction of the  $S_{11}$  and  $S_{21}$  coefficients as in (5) and (6) [25].

$$V_1 = S_{21} + S_{11} \quad (5)$$

$$V_2 = S_{21} - S_{11} \quad (6)$$

Assuredly the S-parameters are primarily associated with the effective permittivity and permeability, with this relationship articulated by (7) and (8). Here,  $K_0$  represents the wave vector, quantified as  $\frac{2\pi}{\lambda_0}$  and  $h$  denotes the substrate thickness [25], [26].

$$\mu_{eff} = \frac{2}{JK_0 h} \frac{1-V_2}{1+V_2} \quad (7)$$

$$\varepsilon_{eff} = \frac{2}{JK_0 h} \frac{1-V_1}{1+V_1} \quad (8)$$

Striving to achieve a resonance frequency of approximately 1.5 GHz and following multiple optimization iterations, the proposed design features the SRR unit cell, as depicted in Figures 1(b) and 1(c).

*A novel configuration of a microstrip metamaterial reconfigurable bandstop filter (Amina Aghanim)*

this unit cell is positioned on an FR-4 (lossy) dielectric substrate, possessing a height ( $h$ ) of 1.6 mm, a length ( $L_s$ ) of 15 mm, a relative dielectric permittivity ( $\epsilon_r$ ) of 4.4 F/m, and a tangent loss of 0.025. The geometry highlights various parameters of the split rings ( $L_1, L_2, w, g, s$ ), with Table 1 providing their numerical values, including the split between the two rings ( $s$ ). Additionally, a microstrip line is etched at the lower face of the substrate at its center, featuring a width  $L_w$  and a height ( $t$ ). The simulation, performed using the 3D electromagnetic solver computer simulation technology (CST) microwave studio, utilized the frequency domain solver, with a waveguide port selected as the excitation method.

Following multiple optimizations of the unit cell resonator dimensions, the envisaged structure underwent simulation to attain a resonance frequency that will serve as the operational frequency for the forthcoming circuit model. Figure 2 illustrates the scattering parameters of the unit cell across different frequencies, showcasing that the operational frequency centers around 1.5 GHz. It is noteworthy to mention that negative permittivity and permeability can indeed result in significant losses, unlike metals. To mitigate these losses, various strategies have been employed, including optimizing geometry and incorporating gain. This allows for achieving minimal losses, even reaching zero loss over a broad frequency range and in alternative designs. To explore this, we investigated both permittivity and permeability, as depicted in Figure 3. The plot reveals that the real part of the permeability is negative  $Re(\mu_r) < 0$  from 1.51 to 1.64 GHz, reaching as low as -380. In this frequency range, the orientation of the rings aligns with the magnetic field component. Furthermore, it can be asserted that the real part of the permeability parameter increases below the resonance frequency.

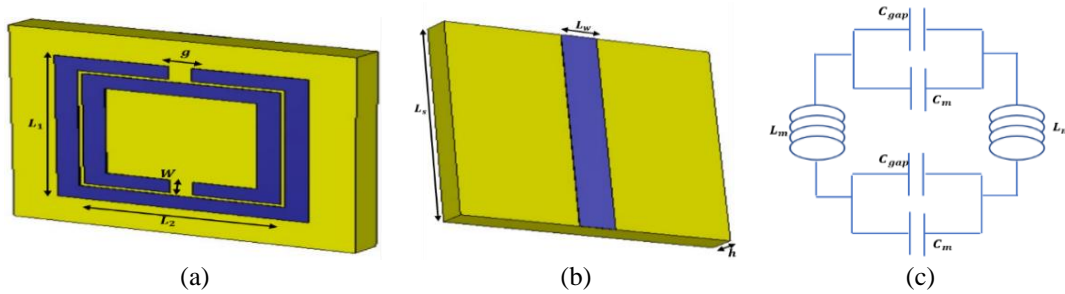


Figure 1. Representation of the metamaterial unit cell geometry and its equivalent circuit

Table 1. Numerical values of the dimensions

Variable	Numerical value (mm)
$L_1$	11
$L_2$	8.6
$g$	1
$w$	1
$s$	0.2
$t$	0.04
$L_w$	2

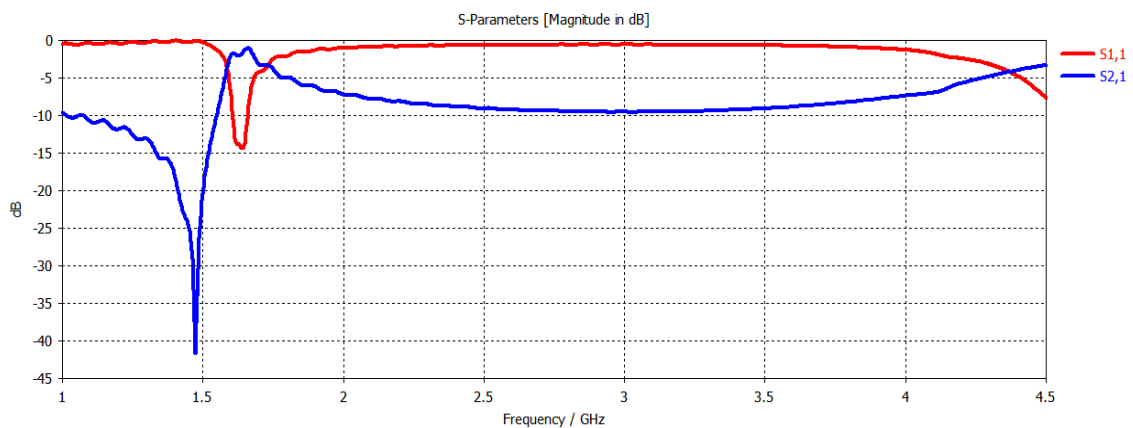


Figure 2. S-parameters of the unit cell in dB

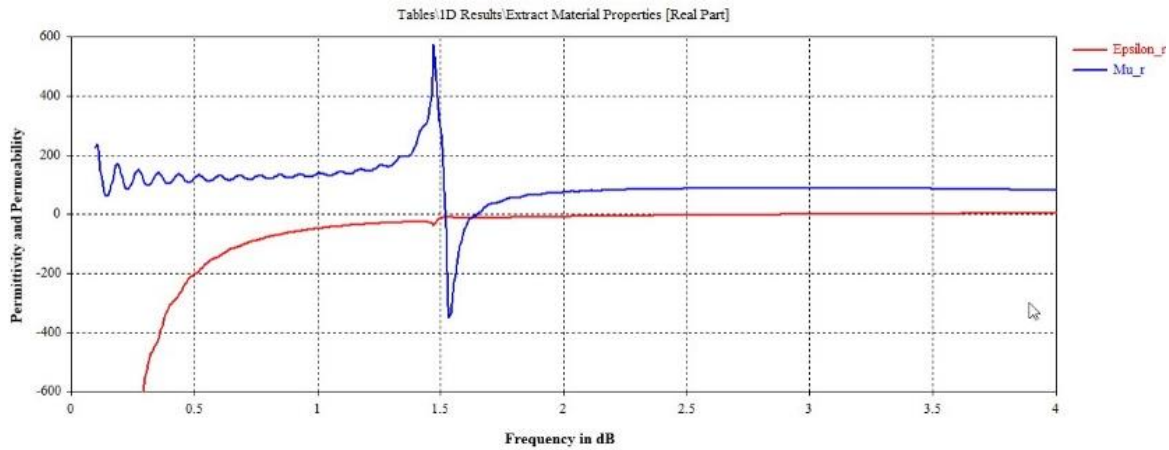


Figure 3. Plot of permittivity and permeability vs frequency

## 2.2. Conception and simulation of bandstop filter with SRRs

Having validated the geometry of the unit SRR cell, we proceeded to conceptualize and simulate a bandstop filter. The proposed geometry for the bandstop filter is visually depicted in Figure 4. Geometry under CST and geometry under ADS, respectively in Figure 4(a) and (b). The structure comprises six rectangular split-ring resonators etched onto the upper face of an FR-4 substrate with a thickness ( $h = 1,6$  mm), a length ( $L_s = 43$  mm), and a width ( $w_s = 28.30$  mm). The microstrip line is characterized by a length ( $L_s$ ) and a width ( $w_s = 2$  mm). The distance between unit cells on the same layer is denoted as ( $S_u$ ) and is equal to 1 mm, while the gap between the microstrip transmission line and each layer is set at 0.15 mm. The SRRs, the microstrip transmission line, and the entire ground plane are implemented using perfect electric conductor materials and are characterized by a height ( $t$ ) of 0.04 mm.

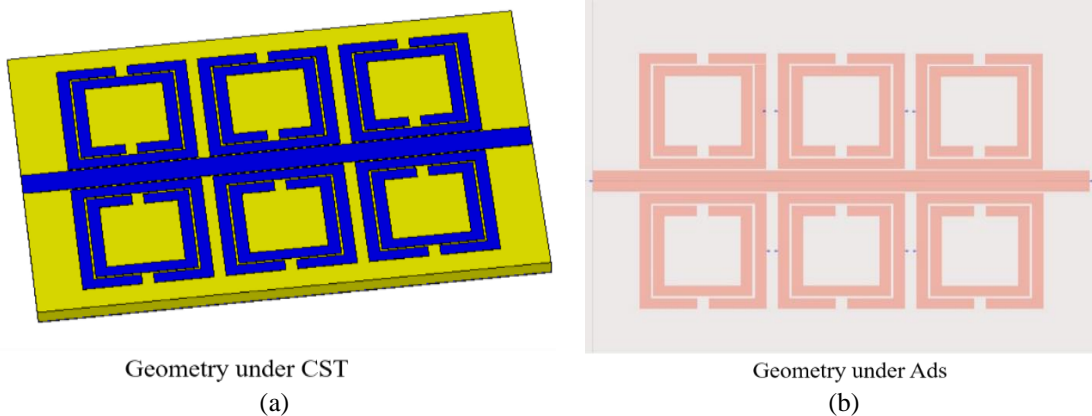


Figure 4. The microstrip bandstop filter geometry (a) CST and (b) ADS

To validate our structure, the simulation was effectuated under two different simulators, CST Studio and ADS Agilent. The results of the S-parameters are depicted in Figure 5. In Figure 5, four curves are presented, encompassing  $S_{11}$  and  $S_{21}$  in both CST and ADS simulations. Within the context of the bandstop filter, the graph illustrates the performance metrics, including acceptable attenuation in the rejected band, a well-matched input impedance level with a reflection coefficient below -18 dB, and a modest -0.5 dB insertion loss. Notably, exceptional electrical performance is evident in both passbands, featuring a rejection level extending to -35 dB in the stop band. The fractional bandwidth spans 17.5%, ranging from 1.49 to 1.79 GHz, with the center frequency positioned precisely at 1.6 GHz. Furthermore, the proximity of the parameter's curves in both simulators highlights the agreement between the two simulators, with only a slight deviation of approximately 20 dB in the rejection level observed in ADS.

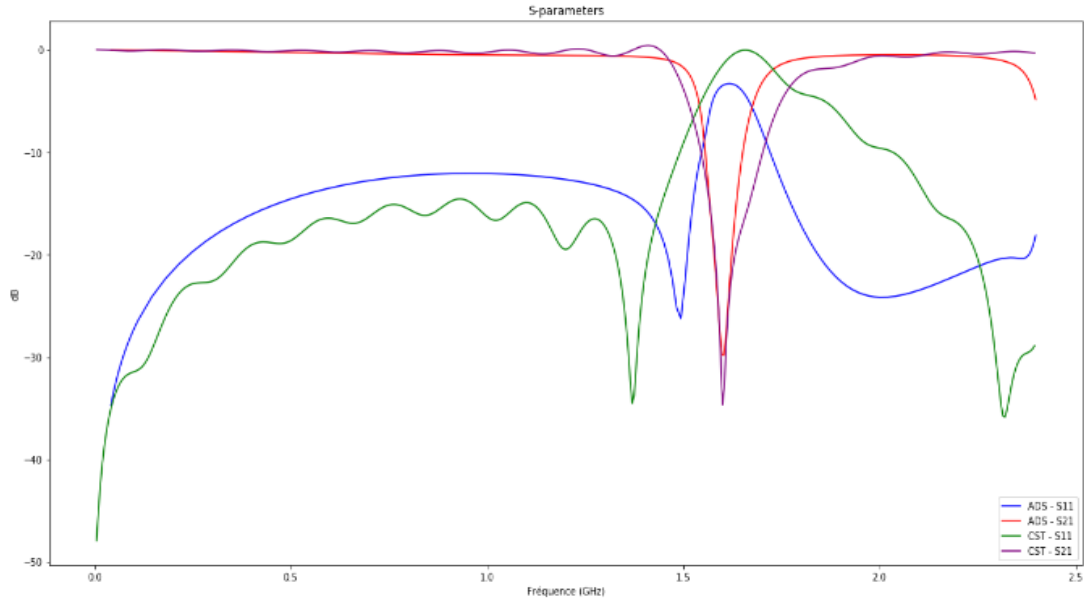


Figure 5. Comparative analysis of S-parameters in CST and ADS

### 2.3. Fabrication and test of the bandstop filter with SRRs

To authenticate the obtained results, the simulated structure was physically fabricated, as illustrated in Figure 6(a), and subsequently tested. The testing process involved the use of the GS-320 vector network analyzer (VNA), specifically designed for on-site applications within a frequency range of 23 to 6,200 MHz. In Figure 6(b), presenting the  $S_{11}$  coefficient, the measured results from the GS-320 align remarkably well with the simulated ones, particularly emphasizing the bandstop behavior despite this alignment, a minor frequency band shift is observed, attributed to the substrate's characteristics during fabrication, which exhibited slight variations in values.

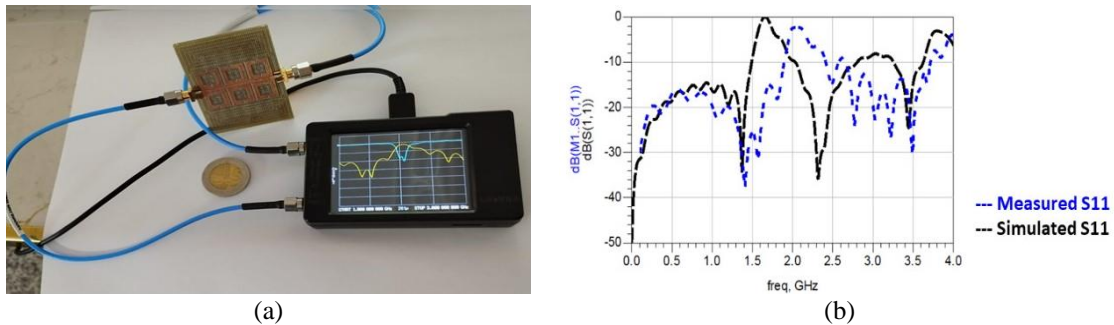


Figure 6. Validation step (a) prototype filter implementation and (b) comparison between simulated and measured results

## 3. RECONFIGURABLE BANDSTOP FILTER WITH VARACTORS

### 3.1. Varactor diode model

To ensure the adaptability of the discussed filter, varicap diodes are incorporated, leveraging their unique properties to govern bandwidth flexibility. Exploiting varactor diodes inherent characteristics, where capacitance dynamically adjusts with applied inverse voltage bias, facilitates the desired reconfigurability of the bandwidth. The objective is to seamlessly integrate four varicap diodes into the prototype of the bandstop filter. For modeling bandwidth reconfigurability in the metamaterial bandstop filter with varactor diodes, the SMV2019 model has been chosen as the variable capacitance element. Employing reference data from Skyworks, we apply  $V_{in}$  levels ranging from 0 to 20 V, resulting in a variable capacitive response spanning from 0.3 to 2.22 pF, which is adapted to the structure of the filter under consideration.

### 3.2. Design and implementation of the SMV2019 varactor

The simplified equivalent circuit of the varactor diode SMV2019 is depicted in Figure 7 where it was conceptualized under ADS simulator, where  $L_s$  is set at 0.7 nH and  $R_s$  at 4.8  $\Omega$ , representing the inductance and series resistance of the device, respectively.  $C_p$  denotes the capacitance and its value changes due to the reverse bias between the anode and cathode of the varactor diode.

The design of the polarization circuit, depicted also in Figure 7, aims to establish effective isolation between the DC and RF components. The conceptualization was validated through simulation, as demonstrated in Figure 8. The  $S_{21}$  coefficient in this figure serves as a clear indicator of the achieved isolation within the frequency band spanning from 2.3 to 2.7 GHz, where the insertion loss achieved -105 dB. The simulation results affirm the circuit's ability to separate and isolate the DC and FR components, confirming its effectiveness in maintaining the desired characteristics within the specified frequency range. After establishing the varicap diode model and its associated polarization circuit, both components were incorporated into the geometry of the SRR bandstop filter as depicted in Figure 9.

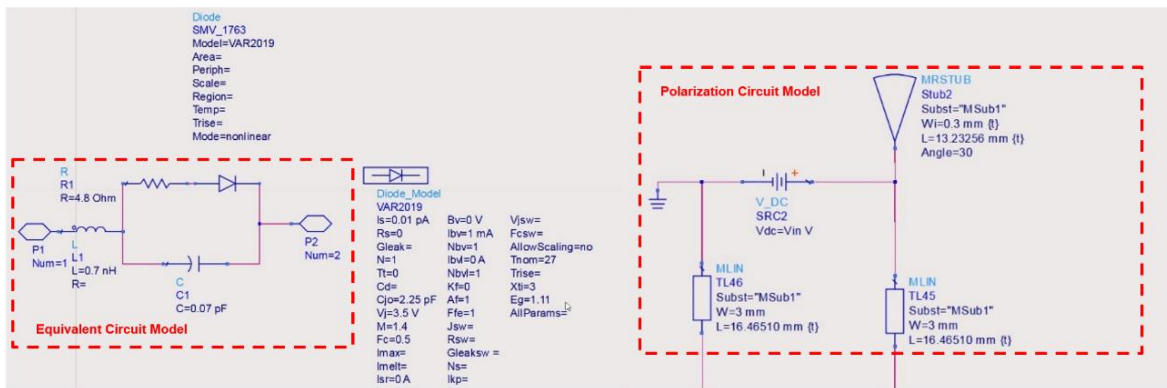


Figure 7. Equivalent circuit of the SMV2019 and its polarization circuit

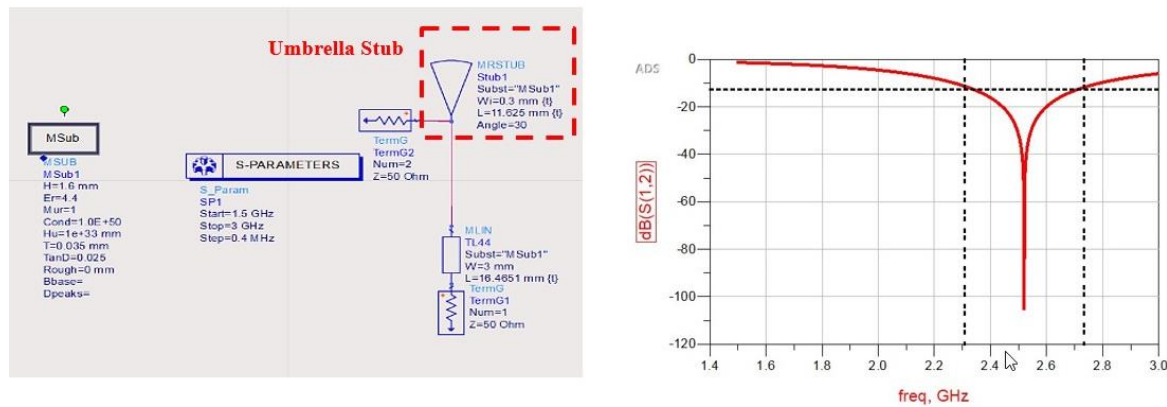


Figure 8. The polarization circuit with umbrella stub, and its  $S_{12}$  coefficient in dB

### 3.3. Results illustration

In examining the results presented in Figure 10, the dynamic behavior of the  $S_{21}$  coefficient in response to changes in inverse voltage bias is evident, showcasing a substantial reconfiguration of the bandwidth. Specifically, the  $S_{21}$  values, initially ranging from 1.65 to 2.08 GHz under  $V_{in} = 0 V$ , have transitioned to a broader bandwidth of 2.05 to 2.45 GHz when  $V_{in} = 20 V$ . An intriguing observation lies in the sensitivity of the Rb1 (first rejected band) to changes in the variable capacitance, as demonstrated by its more pronounced response. Operating below -3 dB, the Rb1 band exhibits a significant shift at 2.05 GHz, characterized by a reverse bias voltage of 6 V and  $C_p = 0.55$  pF, resulting in a tuning range of 1.4 GHz. This tuning effect is further highlighted by the distinct ranges of the Rb1 and Rb2 (second rejected band), with Rb1 spanning from 1.65 to 2.2 GHz and Rb2 extending from 2.35 to 2.55 GHz.

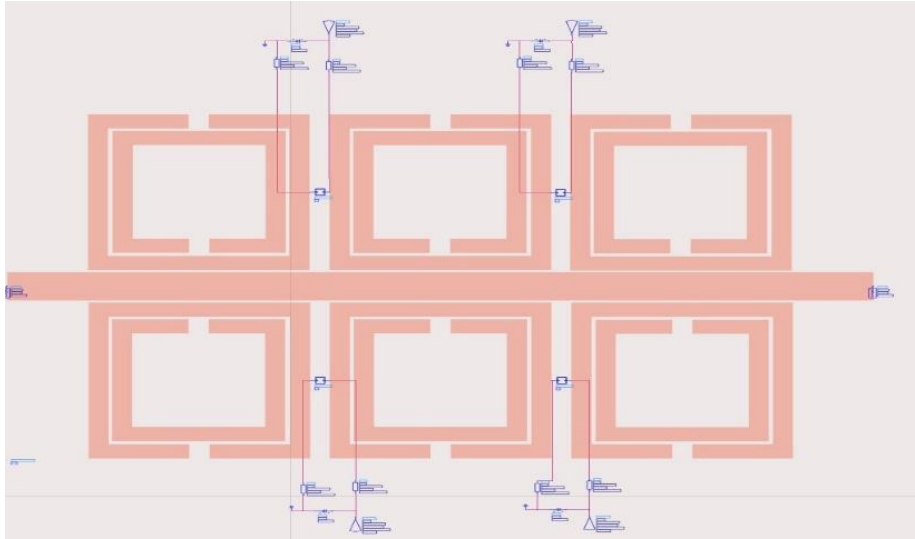


Figure 9. Reconfigurable bandstop filter with four varactor diodes geometry

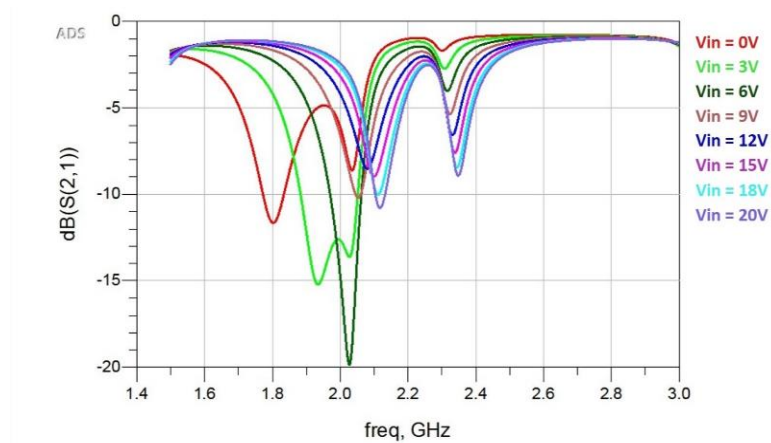


Figure 10. The  $S_{21}$  performances of the reconfigurable filter

The dynamic interplay between the variable capacitance and the resultant shifts in resonant frequencies underscores the efficiency of integrating varactor diodes and their associated polarization circuit in achieving the desired reconfigurability within the bandstop filter. The principal aim in introducing varactor diodes to these configurations was to meticulously observe and analyze the nuanced behavior of bandwidth reconfigurability. This goal has been unequivocally realized, evident in the pronounced variations discerned in the obtained results. This transformative integration of varactors imparts an elevated functionality to the structure, enabling its seamless incorporation into diverse applications. This obviates the need for developing additional structures aimed at rejecting bands, a task adeptly accomplished by the reconfigurable filter itself.

#### 4. CONCLUSION

In conclusion, this article undertakes a comprehensive exploration of a microstrip metamaterial reconfigurable bandstop filter. The investigation initiates a meticulous evaluation of the SRR unit cell, leading to the conception and simulation of a bandstop filter featuring SRRs. Subsequent stages involve the fabrication and testing of the considered structure, confirming the successful realization of the proposed design. The study seamlessly transitions into the reconfigurable aspect, ingeniously transforming the same bandstop filter with SRRs into a reconfigurable bandstop filter using varactors. The incorporation of varactor diodes is thoroughly addressed through modeling, and the ensuing conception and simulation of the reconfigurable filter showcase the adaptability of the design.

Accordingly, the results attest to the successful reconfiguration of the bandstop characteristics, validating the versatility and functionality of the varactor-enhanced design. The dynamic interplay between variable capacitance and shifts in resonant frequencies vividly underscores the efficiency of integrating varactor diodes and their associated polarization circuit in achieving the desired reconfigurability within the bandstop filter. The primary goal of introducing varactors to these configurations was to observe and analyze the nuanced behavior of bandwidth reconfigurability, a goal unequivocally realized as evidenced by the pronounced variations discerned in the obtained results. This transformative integration of varactors imparts elevated functionality to the structure, enabling seamless incorporation into diverse applications. Importantly, it eliminates the need for developing additional structures aimed at rejecting bands, a task adeptly accomplished by the reconfigurable filter itself. From perspectives, our upcoming goal is to control the reconfigurability of the bandwidth of the filter, with an algorithm, where its outputs are the voltage bias of the varactor diodes based on the specifications dictated as inputs of the algorithm.

## REFERENCES




- [1] A. Kadiri, A. Tajmouati, J. Zbitou, and A. Lakhssassi, "A low-cost dual bandpass planar filter for WiMAX and mobile communications," *Indonesian Journal of Electrical Engineering and Computer Science (IJECS)*, vol. 33, no. 2, pp. 757–766, Feb. 2024, doi: 10.11591/ijeecs.v33.i2.pp757-766.
- [2] H. Landaluce, L. Arjona, A. Perallos, F. Falcone, I. Angulo, and F. Muralter, "A review of IoT sensing applications and challenges using RFID and wireless sensor networks," *Sensors (Switzerland)*, vol. 20, no. 9, Apr. 2020, doi: 10.3390/s20092495.
- [3] S. H. Shah and I. Yaqoob, "A survey: internet of things (IoT) technologies, applications and challenges," in *2016 4th IEEE International Conference on Smart Energy Grid Engineering, SEGE 2016*, Aug. 2016, pp. 381–385, doi: 10.1109/SEGE.2016.7589556.
- [4] H. Islam, S. Das, T. Bose, and T. Ali, "Diode based reconfigurable microwave filters for cognitive radio applications: A review," *IEEE Access*, vol. 8, pp. 185429–185444, 2020, doi: 10.1109/ACCESS.2020.3030020.
- [5] F. Liu *et al.*, "Seventy years of radar and communications: the road from separation to integration," *IEEE Signal Processing Magazine*, vol. 40, no. 5, pp. 106–121, Jul. 2023, doi: 10.1109/MSP.2023.3272881.
- [6] D. Moss, "RF and microwave photonic high bandwidth signal processing based on Kerr micro-comb sources," *Preprint*, pp. 1–41, Jul. 2020, doi: 10.36227/techrxiv.12665609.v2.
- [7] B. Nasiri, A. Errkik, and J. Zbitou, "Microstrip band-stop filter based on double negative metamaterial," *International Journal of Electrical and Computer Engineering (IJECE)*, vol. 12, no. 2, pp. 1579–1584, Apr. 2022, doi: 10.11591/ijece.v12i2.pp1579-1584.
- [8] C. W. Tang, C. H. Yang, and J. S. Liao, "Design of planar wide-stopband bandstop filters with extra-high attenuation," *IEEE Transactions on Circuits and Systems II: Express Briefs*, vol. 69, no. 3, pp. 1039–1043, Mar. 2022, doi: 10.1109/TCSII.2021.3137667.
- [9] C. Li, Z. H. Ma, J. X. Chen, M. N. Wang, and J. M. Huang, "Design of a compact ultra-wideband microstrip bandpass filter," *Electronics (Switzerland)*, vol. 12, no. 7, Apr. 2023, doi: 10.3390/electronics12071728.
- [10] A. Bembarca, L. Setti, A. Tribak, H. Tizyi, and M. El Ouahabi, "A novel wideband beamforming antenna for 5G applications by eliminating the phase shifters and crossovers from the butler matrix," *Progress in Electromagnetics Research C*, vol. 133, pp. 51–63, 2023, doi: 10.2528/PIERC23020703.
- [11] B. Nasiri, A. Errkik, J. Zbitou, A. Tajmouati, L. El Abdellaoui, and M. Latrach, "A new compact and wide-band band-stop filter using rectangular SRR," *TELKOMNIKA (Telecommunication Computing Electronics and Control)*, vol. 16, no. 1, pp. 110–117, Feb. 2018, doi: 10.12928/TELKOMNIKA.v16i1.7578.
- [12] N. S. Kumar, K. C. B. Naidu, P. Banerjee, T. A. Babu, and B. V. S. Reddy, "A review on metamaterials for device applications," *Crystals*, vol. 11, no. 5, May 2021, doi: 10.3390/cryst11050518.
- [13] L. Wu and Y. S. Lin, "Flexible terahertz metamaterial filter with high transmission intensity and large tuning range for optical communication application," *Physica E: Low-Dimensional Systems and Nanostructures*, vol. 146, Jan. 2023, doi: 10.1016/j.physe.2022.115563.
- [14] Y. I. A. Al-Yasir, N. O. Parchin, R. A. Abd-Alhameed, A. M. Abdulkhaleq, and J. M. Noras, "Recent progress in the design of 4G/5G reconfigurable filters," *Electronics (Switzerland)*, vol. 8, no. 1, Jan. 2019, doi: 10.3390/electronics8010114.
- [15] A. Bembarca, L. Setti, A. Tribak, H. Nachouane, and H. Tizyi, "Frequency tunable filtenna using defected ground structure filter in the sub-6 GHz for cognitive radio applications," *Progress in Electromagnetics Research C*, vol. 118, pp. 213–229, 2022, doi: 10.2528/PIERC22011403.
- [16] A. Belmajdoub, M. Jorio, S. Bennani, S. Das, and B. T. P. Madhav, "Design of a compact reconfigurable bandpass filter using interdigital capacitor, DMS slots and varactor diode for wireless RF systems," *Journal of Instrumentation*, vol. 16, no. 11, Nov. 2021, doi: 10.1088/1748-0221/16/11/P11013.
- [17] M. Firmlil and A. Zatni, "Dual-wideband sandwich coupled three-lines bandpass filter based on modified open-stub loaded stepped impedance resonator with improved second harmonic for 5G Wi-Fi/ku-band applications," *Heliyon*, vol. 9, no. 2, Feb. 2023, doi: 10.1016/j.heliyon.2023.e13365.
- [18] N. Krishna V and K. G. Padmasine, "A review on microwave band pass filters: materials and design optimization techniques for wireless communication systems," *Materials Science in Semiconductor Processing*, vol. 154, Feb. 2023, doi: 10.1016/j.mssp.2022.107181.
- [19] B. Gowrish and R. R. Mansour, "A tunable quarter-wavelength coaxial filter with constant absolute bandwidth using a single tuning element," *IEEE Microwave and Wireless Components Letters*, vol. 31, no. 6, pp. 658–661, Jun. 2021, doi: 10.1109/LMWC.2021.3064381.
- [20] I. Shahid, D. Thalakituna, D. K. Karmokar, S. J. Mahon, and M. Heimlich, "Periodic structures for reconfigurable filter design: a comprehensive review," *IEEE Microwave Magazine*, vol. 22, no. 11, pp. 38–51, Nov. 2021, doi: 10.1109/MMM.2021.3102197.
- [21] K. V. Babu, S. Das, G. N. J. Sree, B. T. P. Madhav, S. K. K. Patel, and J. Parmar, "Design and optimization of micro-sized wideband fractal MIMO antenna based on characteristic analysis of graphene for terahertz applications," *Optical and Quantum Electronics*, vol. 54, no. 5, Apr. 2022, doi: 10.1007/s11082-022-03671-2.






- [22] G. Joshi and R. Vijaya, "Multiband, continuously tunable filter in 100–300 GHz range using a two-layer cavity of perforated, all-dielectric metasurfaces," *Optical and Quantum Electronics*, vol. 55, no. 2, Dec. 2023, doi: 10.1007/s11082-022-04307-1.
- [23] L. T. Govindaraman, A. Arjunan, A. Baroutaji, J. Robinson, and A. G. Olabi, "Metamaterials for energy harvesting," in *Encyclopedia of Smart Materials*, Elsevier, 2021, pp. 522–534.
- [24] N. Ullah *et al.*, "Corrigendum to 'A compact complementary split ring resonator (CSRR) based perfect metamaterial absorber for energy harvesting applications' [Eng. Sci. Technol. Int. J. 45 (2023) 101473]," *Engineering Science and Technology, an International Journal*, vol. 45, Sep. 2023, doi: 10.1016/j.jestch.2023.101494.
- [25] B. Nasiri, A. Errkik, and J. Zbitou, "A new design of UHF tag antenna for clothing identification using SRR," *TELKOMNIKA (Telecommunication Computing Electronics and Control)*, vol. 19, no. 6, pp. 1755–1760, Dec. 2021, doi: 10.12928/TELKOMNIKA.v19i6.16964.
- [26] M. Stanley *et al.*, "Determination of the permittivity of transmission lines at milli-kelvin temperatures," *IEEE Access*, vol. 11, pp. 60626–60634, 2023, doi: 10.1109/ACCESS.2023.3286374.

## BIOGRAPHIES OF AUTHORS






**Amina Aghanim**    born in Fes, Morocco, is presently pursuing her Ph.D. at the Polydisciplinary Faculty of Larache, part of Abdelmalek Essaadi University. She earned her master's degree in advanced technologies and embedded systems in 2018. Her current research is focused on the tuning of microwave components and automated control, with a particular interest in applying intelligent methods to the tuning process of complex microwave systems. She can be contacted at email: [amina.aghanim@etu.uae.ac.ma](mailto:amina.aghanim@etu.uae.ac.ma).






**Otman Oulhaj**    born in Tetouan, Morocco in 1981, obtained his Bachelor of Science in electronics from Abdelmalek Essaadi University, Tetouan, in 2004. He then pursued a master's degree in electronics and telecommunication at the same university, completing it in 2012. Following this, he earned his Ph.D. in physics in 2019. Currently, he holds the position of Associate Professor of Electronics and Telecommunication at Abdelmalek Essaadi University, FP of Larache, Morocco, where his expertise lies in the design of microwave electronic circuits. He can be contacted at email: [o.oulhaj@uae.ac.ma](mailto:o.oulhaj@uae.ac.ma).






**Jamal Zbitou**    was born in Fes, Morocco, in June 1976. He received a Ph.D. degree in electronics from Polytech of Nantes, the University of Nantes, Nantes, France, in 2005. He is currently an Associate Professor of Electronics at Abdelmalek Essaadi University ENSA of Tétouan & LABTIC (ENSAT), Morocco. He is involved in the design of hybrid, monolithic, active, and passive microwave electronic circuits. He can be contacted at email: [j.zbitou@uae.ac.ma](mailto:j.zbitou@uae.ac.ma).






**Aziz Oukaira**    received a Ph.D. degree in electrical engineering from UQO (the University of Quebec in Outaouais), QC, Canada, in 2020. He is currently a postdoctoral fellow with the Polystim Neurotechnologies Laboratory, Ecole Polytechnique de Montreal, QC, Canada. His research is oriented toward telecommunications applications, thermal management, rapid prototyping on FPGA, MEMS, microelectronics, thermal aspects in VLSI microsystems, biomedical signal modeling, extraction of thermal measurements, and detection of heat zones invisible to the naked eye for surfaces of integrated systems like IC, SoC and SiP, and parallel architecture platforms for embedded systems. He can be contacted at email: [aoukaira@uottawa.ca](mailto:aoukaira@uottawa.ca).



**Ahmed Lakhssassi**    received the B.Eng. and M.Sc. degrees in electrical engineering from the University of Quebec Trois-Rivieres (UQTR), Trois-Rivieres, QC, Canada, in 1988 and 1990, respectively, and the Ph.D. degree in energy and material sciences from the INRS-Energy, Montreal, in 1995. In 1995, he became a Professor of Electro-thermo-mechanical aspects with the Natural Sciences and Engineering Research Council of Canada (NSERC)-Hydro-Quebec Industrial Research Chair, Department of Electrical Engineering, UQTR. Since 1998, he has been with the University of Quebec in Outaouais (UQO), Gatineau. He is currently a Titular professor and responsible for the (LIMA). He is the author/coauthor of more than 240 scientific publications and research reports and a thesis advisor of 90 graduate and undergraduate students. He is a regular member of the Strategic Alliance in Microsystems of Quebec. He can be contacted at email: [ahmed.lakhssassi@uqo.ca](mailto:ahmed.lakhssassi@uqo.ca).



**Rafik Lasri**    is an associate professor at the Physics Department of the Polydisciplinary FP, Abdelmalek Essaadi University, Morocco. He received the Diploma of Advanced Studies (DAS) in 2007 and the Ph.D. degree in design, analysis, and applications of intelligent systems from the University of Granada, Spain, in 2012. Currently, his research interests include intelligent control, application of artificial intelligence to power system control design, fuzzy logic control, control systems engineering, machine learning, wireless computing, and data mining. He published one research book, 4 book chapters, 25 research papers in different international conferences, and 17 research papers published in various SCI and Scopus-indexed international journals. He can be contacted at email: [r.lasri@uae.ac.ma](mailto:r.lasri@uae.ac.ma).